JBC COMMUNICATION

A side-by-side biophysical comparison of five single-domain antibody scaffolds used for synthetic display libraries

Received for publication, October 22, 2025, and in revised form, March 30, 2026 Published, Papers in Press, May 14, 2026
https://doi.org/10.1016/j.jbc.2026.113155

Marlene Rauschmayer[‡], Mustafa Abdellatif[‡], Anna Chubanova, Natascia Leonardi, Anna Beatrice Preinsberger, Jonathan Schwach, and Andreas Stengl[*]

From the Faculty of Biology, Human Biology and BioImaging, LMU Munich, Planegg-Martinsried, Germany

Reviewed by members of the JBC Editorial Board. Edited by Karen Fleming

The development of complex antibody therapeutics requires building blocks with high binding specificity, favorable biophysical traits, and a high degree of humanness. Single-domain antibodies (sdAbs) have emerged as promising candidates due to their small size, stability, and versatility. While originally derived from camelids and cartilaginous fish, humanized and human sdAbs are now accessible *via* synthetic libraries and AI/Ml tools. Multiple sdAb phage display libraries have been created using different scaffolds, but systematic comparison is difficult due to varying methodologies. In this study, we report a side-by-side evaluation of five sdAb scaffolds frequently used in synthetic display libraries. Using sequence analysis, biophysical assays, and AlphaFold-based structure prediction, we evaluated performance across key parameters, including humanness, expression yield, hydrophobicity, monomericity, stability, and display efficiency. Analyzed camelid sdAbs exhibited superior biophysical traits, but the lowest degree of humanness. On the other hand, analyzed sdAbs based on human or humanized VHs show close sequence homology to human germline sequences, but limitations in biophysical traits. Furthermore, we observed that mutations aimed at improving stability or humanization compromised biophysical properties. Our findings underline the complexity of multi-parameter optimization of sdAbs. Simultaneously, they highlight the continued value of synthetic display libraries for application-focused discovery of sdAbs for advanced therapeutic antibody formats.

Since the approval of the first monoclonal antibody nearly 4 decades ago, therapeutic antibodies have become a cornerstone of targeted medicine (1). Antibodies have evolved from immune-derived proteins into modular platforms that can be engineered, reformatted, or functionalized into advanced therapeutics such as multispecific antibodies (2, 3), antibody-drug conjugates (4, 5), or engineered immune cells (6).

Numerous antibody-derived or synthetic binder formats have been developed to preserve or mimic this binding capability (7, 8). Common truncated formats include Fab (Fragment antigen-binding) and scFv (single-chain Fragment variable). While scFvs offer structural simplicity and small size, the lack of CL/CH1 domains and stabilizing disulfide bonds often results in instability (9–11).

Engineered scFv variants (12), alternative scaffolds (7), and AI/Ml-designed binders (13) have been introduced to overcome these limitations. Among them, single-domain antibodies (sdAbs) derived from heavy-chain antibodies (hcAbs) in camelids and cartilaginous fish (14) show exceptional promise. Their minimal size and high intrinsic stability make them ideal as universal antibody building blocks.

For therapeutic use, however, human-like sequences are preferred to minimize anti-drug immune responses. Consequently, the discovery of fully human or humanized antibodies has become a major focus (1, 15–17). Typically performed post-discovery, humanization can be laborious and may compromise binding, stability, or yield.

Advances such as *in vitro* display (18, 19) and humanized mice (20) have enabled the generation of fully human antibodies. This approach shifts humanization from an iterative modification performed post-discovery to a preemptive design step, demanding careful scaffold selection and CDR diversity control. For sdAbs, this is particularly challenging since framework residues critically affect monomer stability (21). Nonetheless, several synthetic *in vitro* libraries have successfully addressed this by using rare human VH sequences with intrinsic monomer stability (22–25), by camelizing human VH frameworks (26–28), or by humanizing highly stable camelid VHHs (29). Each approach presents tradeoffs between developability and biophysical robustness.

To help understand how these strategies influence key antibody characteristics, we compared five sdAb scaffolds frequently used in synthetic phage-displayed libraries—spanning human VH to camelid VHH—in parameters such as expression yield, monomericity, hydrophobicity, storage stability, and phage display efficiency.

Results

Analyzed sdAb scaffolds

In this study, we analyzed five sdAb scaffolds previously described for constructing synthetic phage display libraries: HEL4, VHB1a, VHB1ag, hs2dAb, and sdAbD10. These scaffolds span a sequence gradient from human (HEL4) through

‡ These authors contributed equally to this work.
* For correspondence: Andreas Stengl, stengl@biologie.uni-muenchen.de.

murine-humanized (VHB1a, VHB1ag) and camelid-humanized (hs2dAb) to fully camelid (sdAbD10).

HEL4, derived from the human VH germline V3-23/DP-47 (24), is monomeric at concentrations up to 3 mM, with low aggregation and favorable thermal unfolding. Its stability is mediated not by framework mutations but by CDR residues that shield hydrophobic VL-interface regions and a negatively charged triad in CDR1 contributing to monomer stability (30, 31). These features made HEL4 a preferred scaffold for naive sdAb library generation (22, 27).

VHB1a, derived from the humanized HER2-binding Fab 4D5, was optimized through systematic mutagenesis and *in vitro* evolution to enhance monomer stability (32). Although it displayed high structural integrity, delayed SEC retention indicated surface hydrophobicity, which was mitigated in the derivative VHB1ag through three additional framework mutations (28).

sdAbD10, a camelid VHH (29), is intrinsically stable as a monomer, aided by four hallmark residues (Fig. 1*A*, purple rectangles) that increase framework region 2 (FW2) hydrophilicity (33). Its high thermal stability and refolding capacity enable intracellular use, as has been observed for other VHHs (34–36). To reduce immunogenicity, the humanized variant hs2dAb was created by substituting seven residues with their human VH3 counterparts while retaining the hallmark FW2 positions, yielding a stable and high-affinity scaffold (29).

Sequence and structure comparison

We first compared sdAb scaffolds based on sequence and 3D structure. To enable CDR-independent comparison, VHB1a, VHB1ag, hs2dAb, and sdAbD10 were grafted with placeholder CDRs from the HER2-binding IgG trastuzumab, while HEL4 retained its native CDRs due to their role in monomer stability. Alignment to human germline VH3-23/DP-47 highlights framework differences (Fig. 1*B*): HEL4 shows fewest mismatches (IMGT=2, Kabat=0), followed by VHB1a (IMGT=11, Kabat=7), VHB1ag (IMGT=12, Kabat=8), hs2dAb (IMGT=11, Kabat=10), and sdAbD10 (IMGT=16, Kabat=15). Variation is densest in FW2 (Fig. 1*A*), consistent with its role in the former VL interface; hydrophilic mutations and aromatic-to-polar substitutions reduce interface hydrophobicity and, together with CDR3 folding, shield exposed

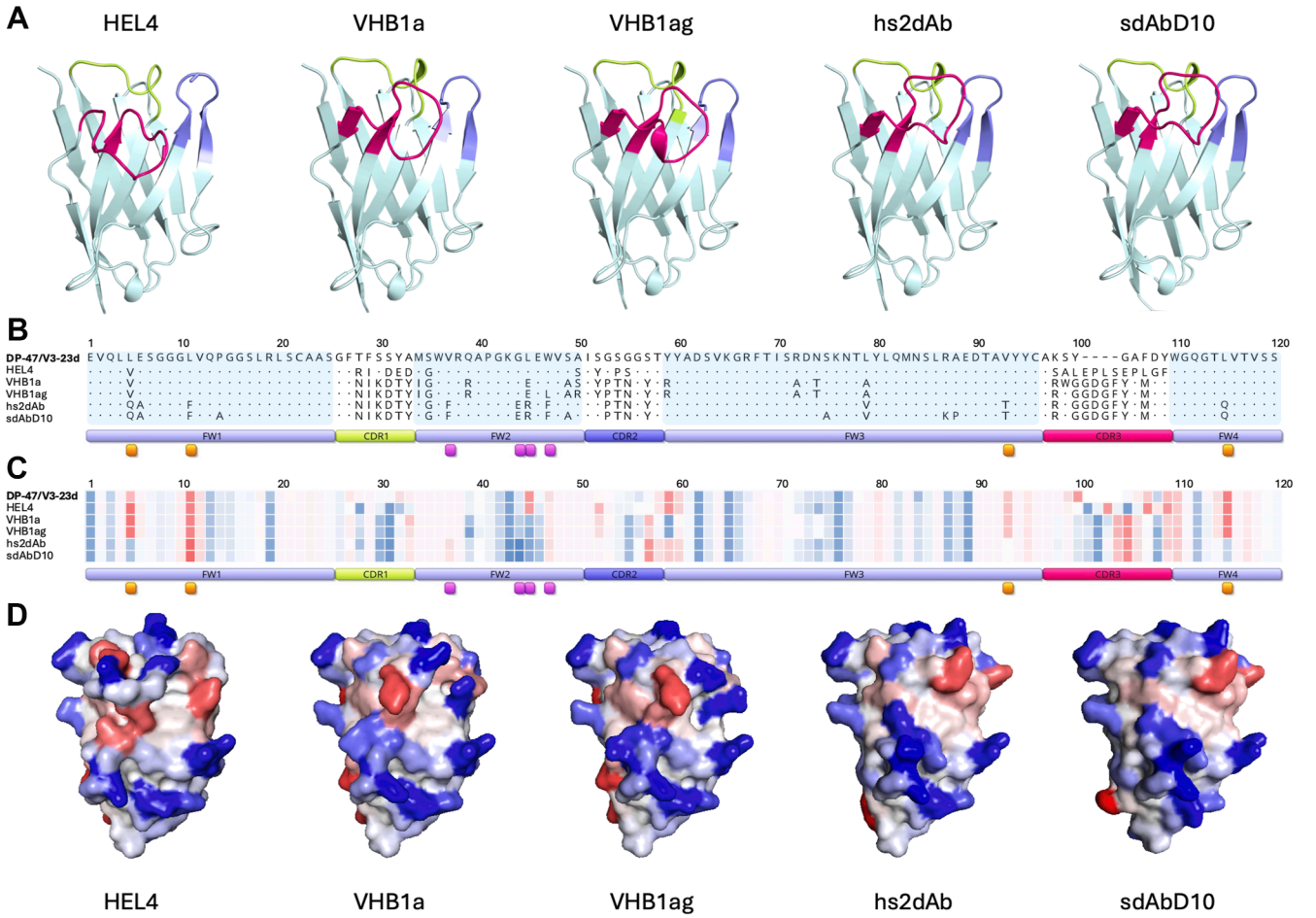

Figure 1. Comparison of sequence, structure, and surface hydrophobicity of sdAb scaffolds. *A*, predicted 3D structures (AlphaFold3) with CDR1–3 highlighted (*yellow*, *purple*, *magenta*; IMGT definition) *B*, amino acid sequence alignment to reference DP47/VH3-23days (human germline). Matches to reference are shown as dots. *C*, per-residue predicted contextual aggregation propensity (A3D score, Aggrescan3D) mapped onto the sequence and colored by A3D score (colors range from *blue* (low: −2.35) to *red* (high: 1.95)). *D*, surface representation of predicted 3D structures (orientation as shown in *A*), colored by A3D score according to (*C*).

sites (37, 38). Both VL interface and CDR3 influence CDR loop arrangement, suggesting backbone sequences affect monomer stability in CDR-dependent and independent ways. AlphaFold3 predictions (Fig. 1*A*) show HEL4's CDR3 folds over the VL interface, burying hydrophobic sites; this is lost when CDRs are replaced with 4D5 sequences (Fig. S2*A*). VHB1a and VHB1ag show less compact CDR3 folding, while camelid-derived hs2dAb and sdAbD10 with identical CDRs show minimal folding. Notably, HEL4's predicted folded CDR3 contrasts its X-ray structure (24), where dimerization restricts folding and buries W52.

Predicted surface hydrophobicity

To assess how framework sequences and conformations influence surface hydrophobicity, we used Aggrescan3D (A3D) (39, 40) to predict aggregation propensity and solubility from 3D structures, yielding residue-specific A3D-scores based on biochemical properties, surface exposure, and structural context. Projecting these scores onto 2D sequences (Fig. 1*C*) revealed that all sdAb scaffolds have less aggregation-prone CDR1 and FW2 than human germline VH3-23/DP-47 (AVG_FW2: VH3-23/DP-47 = −0.16; HEL4 = −0.18; VHB1a = −0.44; VHB1ag = −0.49; hs2dAb = −0.52; sdAbD10 = −0.51). A second aggregation-prone region at the CDR2/FW3 transition is more pronounced in hs2dAb and sdAbD10, likely due to grafting of the 4D5 CDR2. Four isolated residues (alignment positions 5, 11, 93, 115 (Fig. 1, *B* and *C*, orange rectangles) also showed high aggregation scores, three of which are less aggregation-prone in camelid sdAbs. *In silico* V5Q and L115Q mutations in VHB1a reduced the average A3D score (−0.28 → −0.34), suggesting these residues influence solubility.

3D analysis of the former VL interface (Fig. 1*D*) highlights the interplay of FW2 residues and CDR3 conformation. HEL4 lacks hydrophilic FW2 mutations but shields the interface *via* an overlapping CDR3. VHB1a and VHB1ag have polar FW2 patches, yet their CDR3 tyrosine is exposed against the interface. hs2dAb and sdAbD10 have more hydrophilic FW2, with CDR3 not folded over. Rotated views further illustrate HEL4 CDR3 folding and exposure of CDR3 tyrosine in VHB1a/VHB1ag (Fig. S1*B*). Aggregation-prone residues in FW1 (pos. 5) and FW4 (pos. 115) are present on the side-face of HEL4, VHB1a, and VHB1ag but absent in hs2dAb and sdAbD10.

Yields of sdAbs purified from cytoplasm and periplasm

sdAbs are routinely expressed in bacteria. Their intradomain disulfide bond favors periplasmic expression, yet several sdAbs can be produced in the cytoplasm at high yields and remain functional in eukaryotic cytoplasm (10, 29, 34, 36). We systematically compared IMAC-purified yields of five sdAb scaffolds from periplasm and cytoplasm (Fig. 2). Periplasmic yields were highest for HEL4 (9.2 mg/L), followed by hs2dAb (4.4 mg/L), VHB1a (2.3 mg/L), sdAbD10 (1.4 mg/L), and VHB1ag (0.15 mg/L). VHB1ag mutations reduced yield, whereas humanization of sdAbD10 to hs2dAb increased it. Cytoplasmic yields were highest for sdAbD10 (39.5 mg/L), followed by hs2dAb (20.6 mg/L), VHB1a (4.3 mg/L), and HEL4 (3.3 mg/L); VHB1ag could not be purified. The high cytoplasmic yields of sdAbD10 and hs2dAb reflect the specific selection for intracellular stability (29). Interestingly, hs2dAb yields were lower than sdAbD10 in the cytoplasm but higher in the periplasm, suggesting reduced folding speed or stability upon humanization (41, 42).

Biophysical properties of periplasmic and cytoplasmic sdAb preparations

Monomericity and aggregation

To investigate folding efficiency, protein stability, and solubility, we performed a comparative characterization of sdAbs purified from the periplasmic and cytoplasmic space. As a first characteristic, we analyzed monomericity and aggregation *via* analytical size exclusion chromatography (aSEC) after IMAC (Fig. 3). HEL4 isolated from the periplasm is mostly monomeric with a minor extent of higher molecular weight species (HMWS), while the cytoplasmic preparation contains more HMWS (11.0%). VHB1a shows noticeable aggregation with HMWS in both periplasmic (15.4%) and cytoplasmic preparations (10.7%). VHB1ag could not be purified from the cytoplasm, and the periplasmic sample shows high HMWS content (24.7%). hs2dAb and sdAbD10 exhibit only minor HMWS and clear monomer peaks. Thus, humanization of sdAbD10 did not increase HMWS, though overall yield decreased. Notably, cytoplasmic hs2dAb and sdAbD10 peaks show tailing absent in periplasmic samples, suggesting structural differences or local flexibility.

Surface hydrophobicity

As a second biophysical parameter indicative of aggregation potential, we analyzed surface hydrophobicity of IMAC-purified sdAbs by analytical hydrophobic interaction chromatography (aHIC) (Fig. 3). Within the periplasmic preparations, HEL4 (t_R = 12.33 min) and VHB1a (t_R = 12.38 min) showed the longest retention time, corresponding to the highest surface hydrophobicity. VHB1ag harbors mutations to reduce hydrophobicity, reflected in the lower retention time (t_R = 11.52 min) compared to VHB1a. However, a significant peak at lower retention time could represent a multimeric complex burying exposed hydrophobic patches. The high-salt binding buffer used in aHIC could promote this effect compared to the aSEC results. sdAbD10 exhibits the least surface hydrophobicity (t_R = 11.31 min) and humanization to hs2dAb did not increase it (t_R = 11.32 min), likely due to retention of camelid VHH hallmark residues in FW2. The cytoplasmic preparation of HEL4 behaves comparably to the periplasmic sample. For VHB1a, a significant peak at the dead volume might represent larger, non-binding aggregates. Interestingly, cytoplasmic hs2dAb (t_R = 13.50 min) and sdAbD10 (t_R = 13.47 min) shift dramatically to higher retention times, consistent with aSEC tailing, suggesting differences in local folding of surface-exposed regions such as CDRs or FW2.

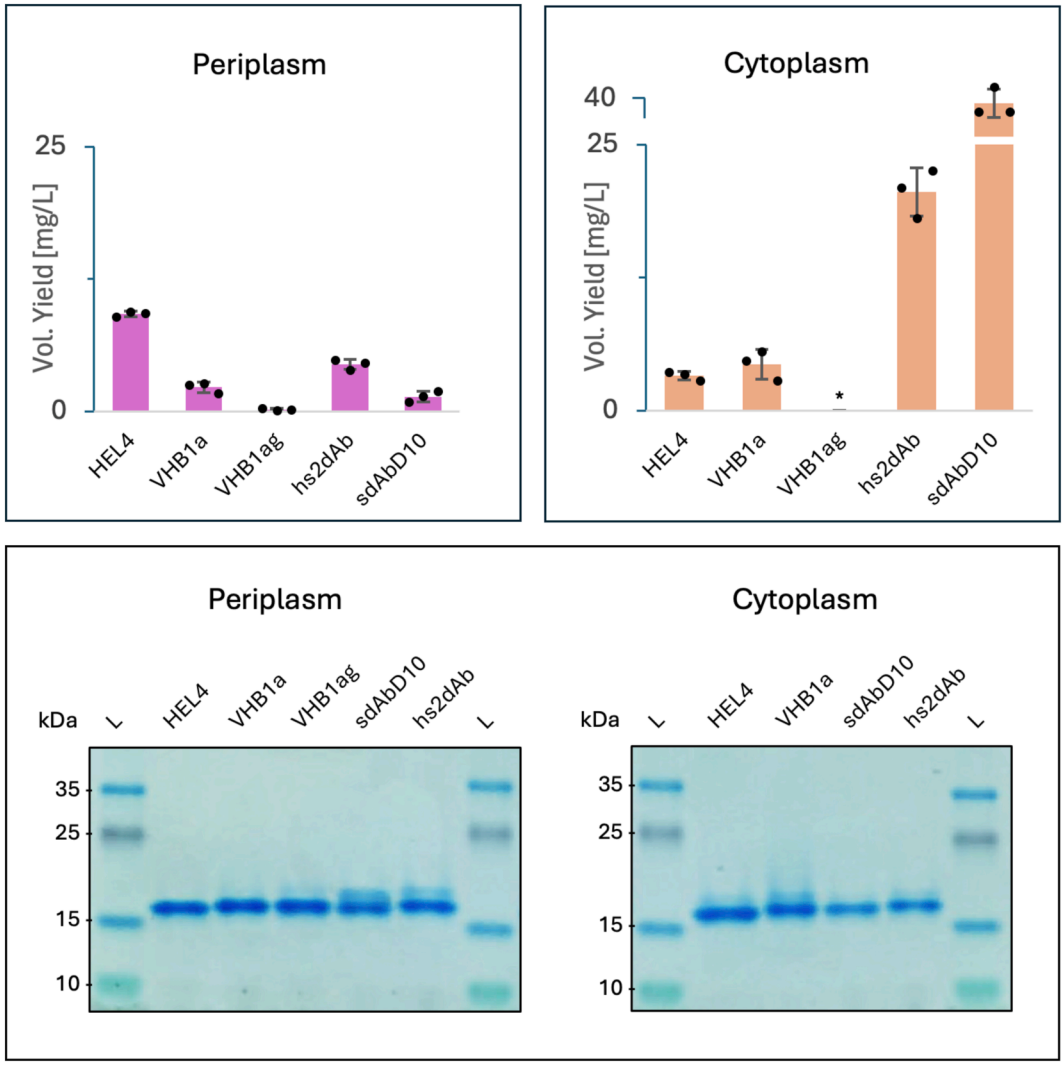

Figure 2. Volumetric yields of IMAC-purified sdAbs from periplasmic and cytoplasmic lysates. Mean ± SD from three independent experiments. Error bars represent the SD of triplicates. Reducing SDS-PAGE confirms purity and expected size (~14 kDa). Asterisk (*) indicates undetectable yield.

Protein stability

As a third biophysical parameter, we analyzed thermal denaturation by differential scanning fluorimetry (DSF) (Fig. 4). For the periplasmic preparations, HEL4 (T_M = 64.4 °C) and VHB1ag (T_M = 64.5 °C) showed the lowest stability. VHB1a has a significantly higher resistance to thermal unfolding (T_M = 73.6 °C) when compared to VHB1ag, suggesting that the mutations introduced to achieve a more hydrophilic surface destabilize the protein fold. The camelid sdAbD10 displays the highest stability (T_M = 82.2 °C), while the humanizing mutations incorporated in its offspring hs2dAb have a destabilizing effect (T_M = 74.1 °C). When isolated from the cytoplasm, HEL4 (T_M = 60.3 °C) and VHB1a (T_M = 71.2 °C) display slightly reduced stability to their respective periplasmic preparations. However, for sdAbD10 (T_M = 62.5 °C) and hs2dAb (T_M = 51.4 °C) we notice a drastic decrease in thermal unfolding stability of ~20 °C. This effect cannot be attributed to global instability since both proteins can be purified at high yields from the cytoplasm and exhibit mostly monomeric peaks in aSEC and aHIC. It is more likely connected to local structural alterations, with one possibility being the lack of an intradomain disulfide bond in the cytoplasmic preparations.

Monomericity, surface hydrophobicity, and storage stability of monomeric sdAbs

To investigate the integrity and stability of monomeric sdAbs post-production, we performed preparative size exclusion chromatography (SEC) and reanalyzed the monomer fractions. Once purified, all sdAb scaffolds showed good monomer stability with HMWS content below 1% except for VHB1ag (HMWS=5.5%) (Fig. 5). This indicates that once formed, the monomers of HEL4, VHB1a, hs2dAb and sdAbD10 are stable under the chosen experimental conditions. The same trend can be observed when analyzed by aHIC (Fig. 5). The retention times are in good agreement with the aHIC data prior to monomer purification (Fig. 3). We again observe a presumably multimeric, less hydrophobic

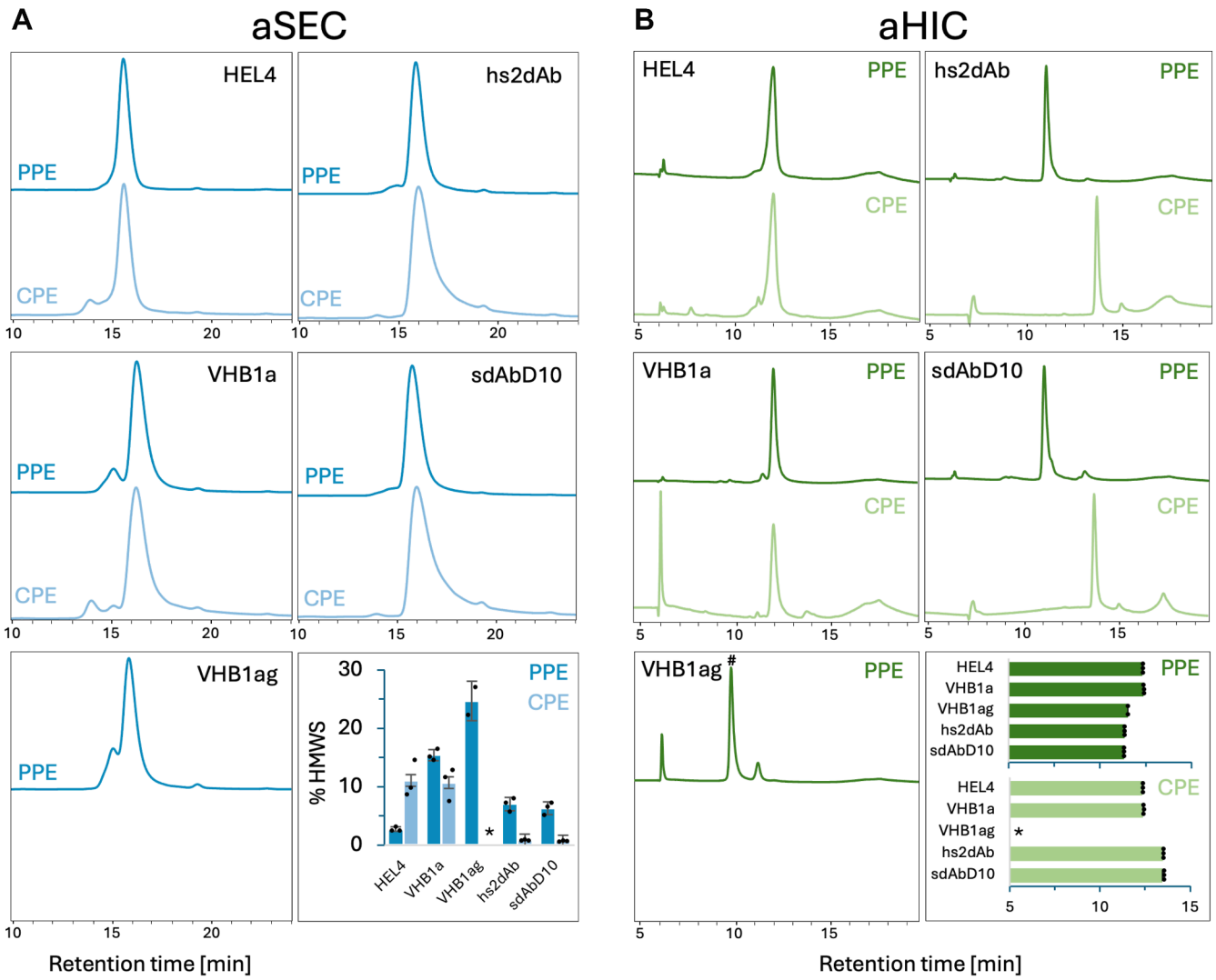

Figure 3. Analytical chromatography of IMAC-purified sdAbs. *A*, aSEC of periplasmic (PPE) and cytoplasmic (CPE) extracts with quantified HMWS content (*bottom right*). *B*, aHIC profiles showing retention times (*bottom right*). A less hydrophobic species is detected for VHB1ag (#). Error bars indicate SD of three biological replicates. Asterisk (*) indicates experiments with no detectable yield.

VHB1ag species that is more pronounced in the high salt conditions of the aHIC analysis than aSEC conditions. Notably, the experimentally determined surface hydrophobicity *via* HIC and the predicted 3D-structure based A3D-scores show strong correlation (r = 0.8, Fig. S2). Finally, we investigated storage stability at 4 °C of the purified sdAbs (Fig. S7). All sdAbs showed good stability for up to 4 weeks except for VHB1ag, which showed a significant loss in total monomer peak area and an increase in low molecular weight species (LMWS) indicative of degradation products.

Efficiency of display on bacteriophage

The sdAbs analyzed in this study have served as universal scaffolds for synthetic phage display libraries. We therefore examined how their frameworks affect phage surface display and overall phage yield. Using a helper phage system sensitive to sdAb expression and periplasmic translocation of sdAb–pIII fusion proteins, we observed efficient display (~50%) for all five sdAbs (Fig. S8). These results indicate that, despite distinct biophysical properties as purified proteins, all scaffolds support comparably efficient phage display.

Discussion

In this study, we conducted a comparative analysis of five sdAb scaffolds spanning sequence homology from human to camelid. We evaluated properties critical for their suitability in synthetic display libraries and as modular elements in therapeutic antibody design, including monomer stability, aggregation propensity, and storage stability.

Sequence and 3D structure analyses point towards distinct mechanisms stabilizing the former VL interface. In analyzed camelid-derived sdAbs (sdAbD10, hs2dAb), polar and aromatic substitutions in FW2 confer stability and permit greater conformational flexibility of CDR3. In contrast, analyzed sdAbs derived from human (HEL4) or humanized sequences (VHB1a, VHB1ag) rely more on CDR3 and polar CDR1 residues for monomer stability.

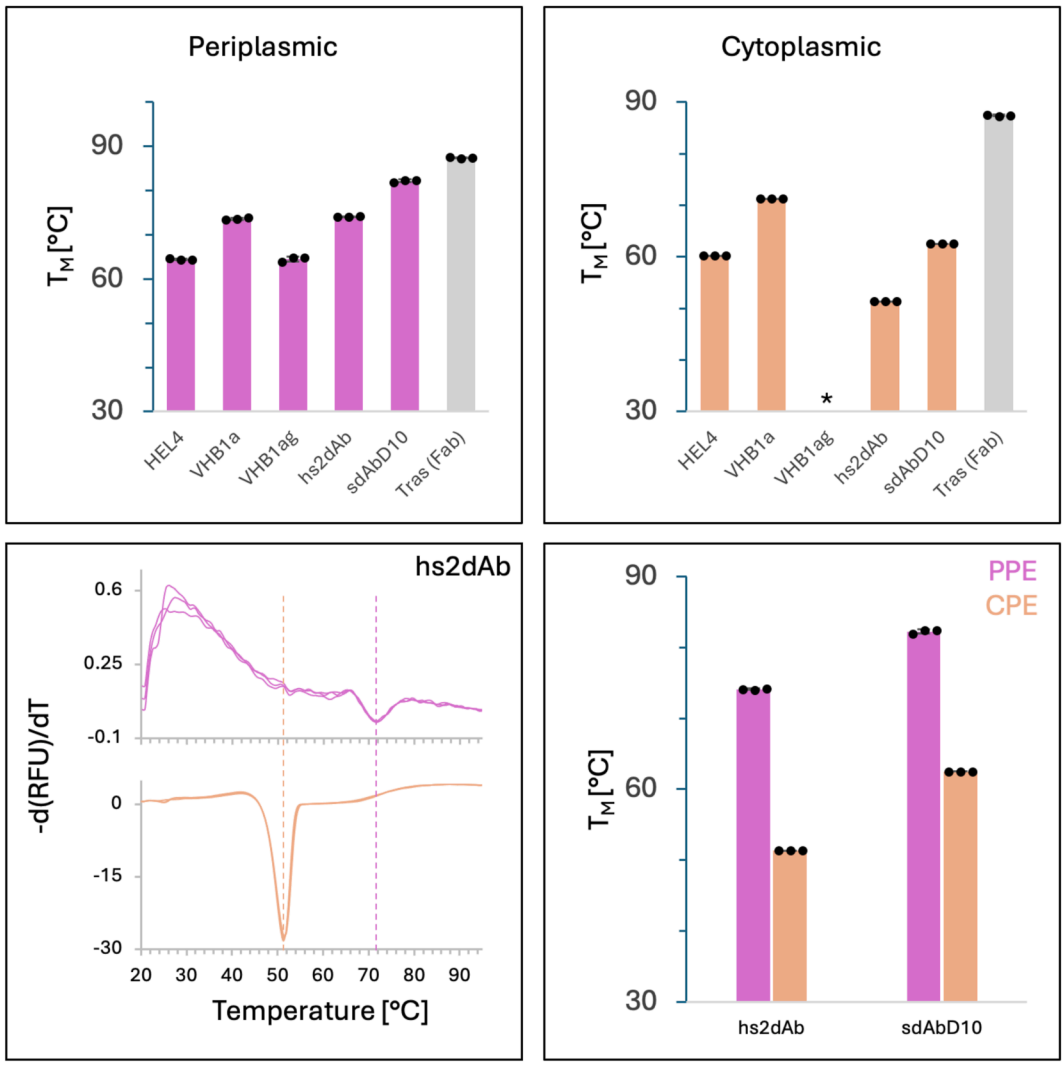

Figure 4. Fold stability of sdAbs analyzed by DSF. *Top panels*: Melting temperatures (T_M) of periplasmic (represented in *magenta*) and cytoplasmic (represented in *orange*) sdAbs (mean ± SD from three technical replicates). *Bottom left*: Representative melting curves for hs2dAb, where the first derivative of SYPRO *Orange* fluorescence is plotted over increasing temperature. Dashed lines correspond to called T_M values. *Bottom right*: Comparison of CPE vs. PPE preparations of hs2dAb and sdAbD10 showing lower T_M in cytoplasmic fractions (mean ± SD from three technical replicates).

Camelid-derived sdAbs analyzed in this study exhibited the highest expression yields, strong monomericity, low surface hydrophobicity, high thermal stability (T_M), and good storage stability. However, their greater deviation from human germline sequences increases immunogenicity risk, and moderate humanization (hs2dAb) reduced yield and fold stability. Human-derived sdAbs displayed less favorable biophysical behavior. VHB1a, for example, showed high T_M but moderate yield and higher hydrophobicity, while hydrophilic mutations in VHB1ag improved solubility but impaired yield and fold stability. HEL4, the most human scaffold, combined high yield, good monomericity, and storage stability with acceptable hydrophobicity and fold stability. Yet, this depends partly on its negatively charged CDR1 and may be sensitive to CDR3 composition, potentially limiting sequence diversity during library construction.

A limitation of this study is the use of fixed CDR sequences to enable scaffold comparison in a largely CDR-independent context. Nonetheless, we cannot fully exclude sequence-specific effects. Future studies should systematically explore CDR sequence tolerance and its influence on scaffold behavior.

When comparing sdAbs isolated from periplasmic *versus* cytoplasmic compartments we observed that analyzed camelid sdAbs (hs2dAb, sdAbD10) displayed reduced fold stability and increased hydrophobicity when expressed cytoplasmically, despite high yields. We hypothesize that altered intradomain disulfide bond formation or CDR exposure contributes to this effect. Understanding this phenomenon could inform future intracellular sdAb applications.

Our findings, consistent with others (43), emphasize the inherent trade-offs in humanization and protein engineering.

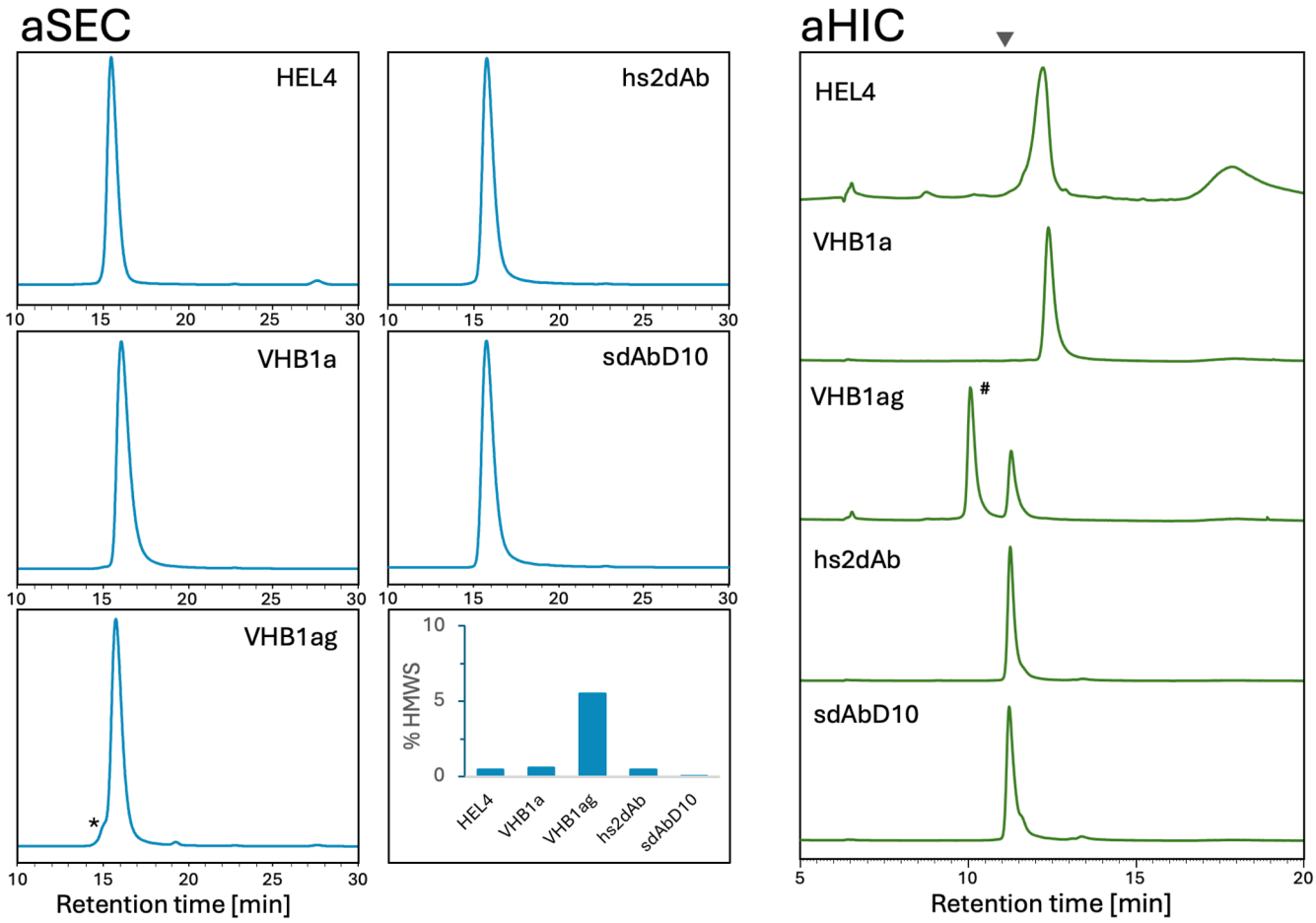

Figure 5. Aggregation and surface hydrophobicity of monomer fractions after preparative SEC. *A*, aSEC profiles showing good monomer stability and low HMWS content; VHB1ag displays minor multimer/aggregate species (*). *B*, aHIC profiles showing surface hydrophobicity differences; HEL4 and VHB1a are most hydrophobic, hs2dAb, sdAbD10, and VHB1ag least. For VHB1ag, a less hydrophobic species is visible (#), which may represent a dimer, consistent with aSEC. Trastuzumab retention time shown (▲).

Optimizing one parameter often compromises another: humanization may increase aggregation, hydrophilic mutations may reduce stability, and backbone alterations can distort CDR conformation (Fig. S9). While advanced computational tools and neural networks will increasingly aid multiparameter optimization, extensive screening remains indispensable. These challenges highlight the continued value of synthetic display libraries, which enable selection of binders with desirable biophysical profiles and defined sequence homology based on shared scaffolds.

Experimental procedures

Recombinant protein expression and purification

Single-domain antibodies were expressed in *Escherichia coli* BL21(DE3) transformed with pET24-based plasmids encoding PelB-FLAG-sdAb-6 × His constructs. Expression was induced with 1 mM IPTG at OD_{600} = 0.6 and continued for 16 h at 18 °C. Periplasmic and cytoplasmic fractions were isolated, clarified by centrifugation, and purified by immobilized metal affinity chromatography (IMAC; HisTrap FF, Cytiva). Peak fractions were buffer exchanged into PBS and further purified by preparative size-exclusion chromatography (Superdex 200 Increase 10/300 Gl, Cytiva). Detailed buffer compositions and chromatography parameters are provided in the Supporting Information.

Analytical chromatography

Analytical SEC and hydrophobic interaction chromatography (HIC) were performed on a Prominence-i LC-2030 system (Shimadzu) using Acclaim-1000 SEC and mAbPac HIC-10 columns (Thermo Fisher Scientific), respectively. Elution was monitored at 220 nm under PBS or phosphate-based mobile phases.

Differential scanning fluorimetry (DSF)

Thermal stability was measured by DSF using SYPRO Orange dye (Invitrogen) on a LightCycler 480 (Roche) with a 20 to 95 °C temperature ramp (0.06 °C/s). Melting temperatures (T_M) were determined from the first derivative of fluorescence intensity.

Phage production and analysis

Bacteriophages were generated by CM13K helper phage superinfection of *E. coli* harboring sdAb-phagemids and

purified by PEG/NaCl precipitation. Phage titers were determined as colony-forming units per mL.

SDS-PAGE and Western Blotting

Phage coat proteins were analyzed by SDS-PAGE and immunoblotting using anti-M13 pIII primary antibody (New England Biolabs) and AlexaFluor647-conjugated secondary antibody (Invitrogen).

Structure prediction and data analysis

sdAb models were generated using AlphaFold3 (https://alphafoldserver.com/) and analyzed for aggregation propensity with Aggrescan3D (https://biocomp.chem.uw.edu.pl/A3D2/). Data were processed in Geneious Prime 2023.2.1 and Microsoft Excel 16.

Comprehensive experimental details are available in the Supporting Information.

Data availability

Supplementary data and detailed methods are available in the Supporting Information. Additional data and materials are available from the corresponding author upon reasonable request.

Supporting information—This article contains Supporting Information.

Acknowledgments—We thank Prof. Dr Heinrich Leonhardt for valuable discussions and generous support with infrastructure.

Author contributions—M. R., M. A., N. L., and A. S. methodology; M. R. and M. A. data curation; M. R. and A. S. visualization; M. R., M. A., and N. L. investigation; M. R., M. A., and A. S. writing - review & editing; M. R., M. A., and A. S. writing - original draft; M. R., M. A., J. S., and A. S. conceptualization; M. R., M. A., A. C., N. L., and A. B. P. formal analysis; A. C. and A. B. P. investigation; A. C., N. L., A. B. P., and J. S. validation; J. S. and A. S. supervision; A. S. data curation.

Funding and additional information—This work was supported by funding from the Bavarian Research Foundation to A. S. and LMU Munich (LMUexcellent Postdoc Support Fund) to A. S.

Conflict of interest—The authors declare that they have no conflicts of interest with the contents of this article.

Abbreviations—The abbreviations used are: A3D, Aggrescan3D; HcAb, heavy-chain antibodies; HIC, hydrophobic interaction chromatography; ScFv, single-chain Fragment variable; SdAbs, Single-domain antibodies; SEC, size exclusion chromatography.

References

1. Crescioli, S., Kaplon, H., Wang, L., Visweswaraiah, J., Kapoor, V., and Reichert, J. M. (2025) Antibodies to watch in 2025. *mAbs* **17**, 2443538
2. Mullin, M., James, M., Winston, H., Justin, G., Nathan, R., and van Heeke, G. (2024) Applications and challenges in designing VHH-based bispecific antibodies: leveraging machine learning solutions. *mAbs* **16**, 2341443
3. Klein, C., Brinkmann, U., Reichert, J. M., and Kontermann, R. E. (2024) The present and future of bispecific antibodies for cancer therapy. *Nat. Rev. Drug Discov.* **23**, 301–319
4. Dumontet, C., Reichert, J. M., Senter, P. D., Lambert, J. M., and Beck, A. (2023) Antibody–drug conjugates come of age in oncology. *Nat. Rev. Drug Discov.* **22**, 641–661
5. Schwach, J., Abdellatif, M., and Stengl, A. (2022) More than toxins-current prospects in designing the next generation of antibody drug conjugates. *Front. Biosci. (Landmark Ed.)* **27**, 240
6. Sterner, R. C., and Sterner, R. M. (2021) CAR-T cell therapy: current limitations and potential strategies. *Blood Cancer J.* **11**, 69
7. Zhang, S., Wu, L., and Dang, M. (2024) Antibody mimetics: the next generation antibody engineering, a retrospective and prospective analysis. *Biotechnol. J.* **19**, e2300532
8. Binz, H. K., Amstutz, P., and Plückthun, A. (2005) Engineering novel binding proteins from nonimmunoglobulin domains. *Nat. Biotechnol.* **23**, 1257–1268
9. Condado-Morales, I., Fabian, D., Waibel, I., Turnbull, O. M., Bhargav, P., Zheng, C., *et al.* (2024) A comparative study of the developability of full-length antibodies, fragments, and bispecific formats reveals higher stability risks for engineered constructs. *mAbs* **16**, 2403156
10. Li, D., Peng, Q., Huang, C., Zang, B., Ren, J., Ji, F., *et al.* (2022) Cytoplasmic expression of nanobodies with formylglycine generating enzyme tag and conversion to a bio-Orthogonal Aldehyde Group in single-domain antibodies. *Methods Mol. Biol.* **2446**, 357–371
11. Jain, T., Sun, T., Durand, S., Hall, A., Houston, N. R., Nett, J. H., *et al.* (2017) Biophysical properties of the clinical-stage antibody landscape. *Proc. Natl. Acad. Sci. U. S. A.* **114**, 944–949
12. Boucher, L. E., Geyer, P. E., Michael, F., Fang, Y., Rupesh, N., Sheng-Jiun, W., *et al.* (2023) "Stapling" scFv for multispecific biotherapeutics of superior properties. *mAbs* **15**, 2195517
13. Vázquez Torres, S., Leung, P. J. Y., Venkatesh, P., Lutz, I. D., Hink, F., Huynh, H.-H., *et al.* (2024) *De novo* design of high-affinity binders of bioactive helical peptides. *Nature* **626**, 435–442
14. Helma, J., Cardoso, M. C., Muyldermans, S., and Leonhardt, H. (2015) Nanobodies and recombinant binders in cell biology. *J. Cell Biol.* **209**, 633–644
15. Waldmann, H. (2019) Human monoclonal antibodies: the benefits of humanization. *Methods Mol. Biol.* **1904**, 1–10
16. Safdari, Y., Safar, F., Mohammad, A., and Khalili, M. (2013) Antibody humanization methods – a review and update. *Biotechnol. Genet. Eng. Rev.* **29**, 175–186
17. Gordon, G. L., Raybould, M. I. J., Wong, A., and Deane, C. M. (2024) Prospects for the computational humanization of antibodies and nanobodies. *Front. Immunol.* **15**, 1399438
18. Jaroszewicz, W., Morcinek-Orłowska, J., Pierzynowska, K., Gaffke, L., and Węgrzyn, G. (2022) Phage display and other peptide display technologies. *FEMS Microbiol. Rev.* **46**, fuab052
19. Bradbury, A. R. M., Sidhu, S., Dübel, S., and McCafferty, J. (2011) Beyond natural antibodies: the power of *in vitro* display technologies. *Nat. Biotechnol.* **29**, 245–254
20. Clarke, S. C., Ma, B., Trinklein, N. D., Schellenberger, U., Osborn, M. J., Ouisse, L. H., *et al.* (2018) Multispecific antibody development platform based on human heavy chain antibodies. *Front. immunol.* **9**, 3037
21. Fernández-Quintero, M. L., Guarnera, E., Musil, D., Pekar, L., Sellmann, C., Freire, F., *et al.* (2024) On the humanization of VHHs: prospective case studies, experimental and computational characterization of structural determinants for functionality. *Protein Sci.* **33**, e5176
22. Rouet, R., Dudgeon, K., Christie, M., Langley, D., and Christ, D. (2015) Fully human VH single domains that rival the stability and cleft recognition of camelid antibodies. *J. Biol. Chem.* **290**, 11905–11917
23. Mandrup, O. A., Friis, N. A., Lykkemark, S., Just, J., and Kristensen, P. (2013) A novel heavy domain antibody library with functionally optimized complementarity determining regions. *PLoS One* **8**, e76834
24. Jespers, L., Schon, O., James, L. C., Veprintsev, D., and Winter, G. (2004) Crystal structure of HEL4, a soluble, refoldable human V(H) single domain with a germ-line scaffold. *J. Mol. Biol.* **337**, 893–903

25. Chen, W., Zhu, Z., Feng, Y., Xiao, X., and Dimitrov, D. S. (2008) Construction of a large phage-displayed human antibody domain Library with a scaffold based on a newly identified highly soluble, stable heavy chain variable domain. *J. Mol. Biol.* **382**, 779–789
26. Lee, N. J., Jung, M., Yang, H. Y., and Shim, H. (2024) A single-domain antibody library based on a stability-engineered human VH3 scaffold. *Sci. Rep.* **14**, 17747
27. Bracken, C. J., Lim, S. A., Solomon, P., Rettko, N. J., Nguyen, D. P., Zha, B. S., *et al.* (2021) Bi-paratopic and multivalent VH domains block ACE2 binding and neutralize SARS-CoV-2. *Nat. Chem. Biol.* **17**, 113–121
28. Ma, X., Barthelemy, P. A., Rouge, L., Wiesmann, C., and Sidhu, S. S. (2013) Design of synthetic autonomous VH domain libraries and structural analysis of a VH domain bound to vascular endothelial growth factor. *J. Mol. Biol.* **425**, 2247–2259
29. Moutel, S., Bery, N., Bernard, V., Keller, L., Lemesre, E., de Marco, A., *et al.* (2016) NaLi-H1: a universal synthetic library of humanized nanobodies providing highly functional antibodies and intrabodies. *eLife* **5**, e16228
30. Nilvebrant, J., Tessier, P. M., and Sidhu, S. S. (2016) Engineered autonomous human variable domains. *Curr. Pharm. Des.* **22**, 6527–6537
31. Perchiacca, J. M., Bhattacharya, M., and Tessier, P. M. (2011) Mutational analysis of domain antibodies reveals aggregation hotspots within and near the complementarity determining regions. *Proteins* **79**, 2637–2647
32. Barthelemy, P. A., Raab, H., Appleton, B. A., Bond, C. J., Wu, P., Wiesmann, C., *et al.* (2008) Comprehensive analysis of the factors contributing to the stability and solubility of autonomous human V_H domains. *J. Biol. Chem.* **283**, 3639–3654
33. Dumoulin, M., Conrath, K., Van Meirhaeghe, A., Meersman, F., Heremans, K., Frenken, L. G. J., *et al.* (2002) Single-domain antibody fragments with high conformational stability. *Protein Sci.* **11**, 500–515
34. Zhang, C., Ötjengerdes, R. M., Roewe, J., Mejias, R., and Marschall, A. L. J. (2020) Applying antibodies inside cells: principles and recent advances in neurobiology, Virology Oncology. *BioDrugs* **34**, 435–462
35. Kirchhofer, A., Helma, J., Schmidthals, K., Frauer, C., Cui, S., Karcher, A., *et al.* (2010) Modulation of protein properties in living cells using nanobodies. *Nat. Struct. Mol. Biol.* **17**, 133–138
36. Rothbauer, U., Zolghadr, K., Tillib, S., Nowak, D., Schermelleh, L., Gahl, A., *et al.* (2006) Targeting and tracing antigens in live cells with fluorescent nanobodies. *Nat. Methods* **3**, 887–889
37. Kuroda, D., and Tsumoto, K. (2023) Structural classification of CDR-H3 in single-domain VHH antibodies in computer-aided antibody design. *Methods Mol. Biol.* **2552**, 61–79
38. Foote, J., and Winter, G. (1992) Antibody framework residues affecting the conformation of the hypervariable loops. *J. Mol. Biol.* **224**, 487–499
39. de Groot, N. S., Castillo, V., Graña-Montes, R., and Ventura, S. (2012) AGGRESCAN: method, application, and perspectives for drug design. *Methods Mol. Biol.* **819**, 199–220
40. Conchillo-Solé, O., de Groot, N. S., Avilés, F. X., Vendrell, J., Daura, X., and Ventura, S. (2007) AGGRESCAN: a server for the prediction and evaluation of "hot spots" of aggregation in polypeptides. *BMC Bioinformatics* **8**, 65
41. Thie, H., Schirrmann, T., Paschke, M., Dübel, S., and Hust, M. (2008) SRP and Sec pathway leader peptides for antibody phage display and antibody fragment production in E. coli. *N. Biotechnol.* **25**, 49–54
42. Steiner, D., Forrer, P., Stumpp, M. T., and Plückthun, A. (2006) Signal sequences directing cotranslational translocation expand the range of proteins amenable to phage display Nature. *Biotechnology* **24**, 823–831
43. Fernández-Quintero, M. L., Anne, L., Franz, W., Victor, G., Andersen, J. T., *et al.* (2023) Assessing developability early in the discovery process for novel biologics. *mAbs* **15**, 2171248